Journal of Zhejiang University-SCIENCE A (Applied Physics & Engineering)
ISSN 1673-565X (Print); ISSN 1862-1775 (Online)
www.zju.edu.cn/jzus; www.springerlink.com
E-mail: jzus@zju.edu.cn

A 2DOF hybrid energy harvester based on combined piezoelectric and electromagnetic conversion mechanisms*

Hong-yan WANG†[1,2], Li-hua TANG[3], Yuan GUO[1], Xiao-biao SHAN[2], Tao XIE[2]

([1]*College of Computer and Control Engineering, Qiqihar University, Qiqihar 161006, China*)

([2]*State Key Laboratory of Robotics and System, Harbin Institute of Technology, Harbin 150001, China*)

([3]*Department of Mechanical Engineering, University of Auckland, Auckland 1010, New Zealand*)

†E-mail: wanghongyan1993@163.com

Received May 4, 2014; Revision accepted July 24, 2014; Crosschecked Aug. 25, 2014

Abstract: This paper presents a two-degree-of-freedom (2DOF) hybrid piezoelectric-electromagnetic energy harvester (P-EMEH). Such a 2DOF system is designed to achieve two close resonant frequencies. The combined piezoelectric-electromagnetic conversion mechanism is exploited to further improve the total power output of the system in comparison to a stand-alone piezoelectric or electromagnetic conversion mechanism. First, a mathematical model for the 2DOF hybrid P-EMEH is established. Subsequently, the maximal power output of the 2DOF hybrid P-EMEH is compared both experimentally and theoretically with those from the 1DOF piezoelectric energy harvester (PEH), 1DOF electromagnetic energy harvester (EMEH), 2DOF PEH, and 2DOF EMEH. Based on the validated mathematical model, the effect of the effective electromechanical coupling coefficients (EMCC) on the maximal power outputs from various harvester configurations is analyzed. The results indicate that for the 2DOF hybrid P-EMEH, although the increase of the power output from one electromechanical transducer will lead to the decrease of the power output from the other, the overall performance of the system is improved in weak and medium coupling regimes by increasing electromechanical coupling. In weak and medium coupling scenarios, the hybrid energy harvester configuration is advantageous over conventional 1DOF or 2DOF harvester configurations with a stand-alone conversion mechanism.

Key words: Vibration, Two-degree-of-freedom (2DOF), Hybrid piezoelectric-electromagnetic conversion, Energy harvesting
doi:10.1631/jzus.A1400124 **Document code:** A **CLC number:** TM619; TN384

1 Introduction

Over the past few years, vibration energy harvesting has attracted much research interest owing to its potential to implement low-cost self-powered wireless sensors. Some methods are commonly pursued to harness electrical energy from ambient vibrations, including electrostatic generation (Lallart *et al.*, 2011), electromagnetic induction (Elvin and Elvin, 2011; Jung *et al.*, 2011), and the piezoelectric effect (Yang *et al.*, 2009; Lumentut and Howard, 2011; Wang *et al.*, 2012; 2014). No matter which method is adopted, the efficiency improvement of a vibration energy harvester involves effort in terms of both bandwidth enlargement and magnitude amplification.

Conventional vibration energy harvesters are usually designed as one-degree-of-freedom (1DOF) models (Williams and Yates, 1996; Roundy *et al.*, 2003; Dutoit *et al.*, 2005), which are efficient near a single resonant frequency. Narrow operating bandwidth is a major challenge for 1DOF vibration energy harvesters (Tang *et al*., 2013). To overcome that drawback, some researchers have considered the use of two-degree-of-freedom (2DOF) models to achieve two close resonances for wider bandwidth. Aldraihem and Baz (2011) and Arafa *et al*. (2011) proposed a

* Project supported by the National Natural Science Foundation of China (No. 51077018), the Heilongjiang Provincial Natural Science Fundation (No. F201219), and the Program for Young Teachers Scientific Research in Qiqihar University (No. 2012k-Z12), China

2DOF piezoelectric energy harvester (PEH) model comprising a piezoelectric harvester and an additional spring-mass system installed between the harvester and the base. The additional spring-mass system served as a dynamic magnifier to enhance the power output and meanwhile achieve a wider bandwidth. Tang and Yang (2012) presented a 2DOF PEH model comprising dual spring-mass-dampers connected in series, where a piezoelectric transducer for power generation was placed between the primary mass and the base, and a parasitic mass connected to the primary mass was used to achieve two close resonant frequencies. Harne (2012) established the mathematical models of a 2DOF electromagnetic energy harvester (EMEH) and a 2DOF PEH, respectively. With these established models, a parametric study was performed to investigate the energy harvesting efficiency of these two types of 2DOF harvesters.

On the other hand, most studies in the energy harvesting field have focused on stand-alone conversion mechanisms (electrostatic, electromagnetic, or piezoelectric). Piezoelectric and electrostatic mechanisms are suitable for small size harvesters in view of their compatibility with standard microelectromechnical systems (MEMS) manufacturing procedure, while electromagnetic mechanisms are more suitable for large size harvesters. In recent studies, the hybrid energy harvesting technology is being increasingly investigated (Khaligh *et al.*, 2008; Wacharasindhu and Kwon, 2008; Challa *et al.*, 2009; Tadesse *et al.*, 2009; Yang *et al.*, 2010; Kim *et al.*, 2012; Shan *et al.*, 2013). Usually, for hybrid energy harvesting, the PEH and EMEH should be on the same scale (for comparable power output), otherwise the hybrid scheme will be meaningless. Tadesse *et al*. (2009) proposed a multimodal energy harvesting device that combines piezoelectric and electromagnetic energy harvesting mechanisms. They found that the electromagnetic transducer could generate much higher power at lower frequencies (the first transversal resonance mode), while the piezoelectric transducer does so at higher frequencies (the second transversal resonance mode). Thus, the combination of the two transducers into a device can generate higher power outputs covering multiple modes. Challa *et al*. (2009) presented a coupled piezoelectric-electromagnetic energy harvesting technique, where two independent energy harvesting mechanisms are coupled to provide higher electrical damping so as to match it better to the mechanical damping in the system for an increased power output. However, questions, such as how the two conversion mechanisms affect each other and how the coupling strengths affect overall performance after combination, have not been properly answered, especially for a multiple DOF energy harvesting system.

This paper proposes a 2DOF hybrid piezoelectric-electromagnetic energy harvester (P-EMEH) system, which aims at not only achieving wider bandwidth but also an increased output by combining piezoelectric and electromagnetic components of comparable macroscopic size. A mathematical model for the 2DOF hybrid P-EMEH system is established. The system parameters for model validation are determined from experiment. The maximal power output from the 2DOF hybrid P-EMEH is compared both experimentally and theoretically with those from other energy harvesting configurations, including 1DOF PEH, 2DOF PEH, 1DOF EMEH, and 2DOF EMEH. The advantage of using the 2DOF hybrid P-EMEH is discussed. Finally, the effect of the effective electromechanical coupling coefficients (EMCC) on the maximal power outputs from various harvester configurations is investigated.

2 Proposed model of 2DOF hybrid P-EMEH

A conventional vibration energy harvester is designed as a 1DOF lumped parameter model. Figs. 1a and 1b show a 1DOF PEH model and a 1DOF EMEH model, respectively. The 1DOF PEH model comprises a mass M_1, spring K_1, damping C_1, and the piezoelectric element. The piezoelectric element is placed between the base and the mass, generating alternating electrical output to power the resistor R_{L1}. The 1DOF EMEH model comprises the mass M_2, spring K_2, and damper C_2, where the magnetic mass M_2 vibrates through the axis of a wound coil. The coil is moving together with the base motions and the current is induced in the electromagnetic energy harvesting coil, delivering power to the resistor R_{L2}.

The 1DOF energy harvester model is only efficient near its sole resonant frequency. This drawback of the 1DOF model limits its applicability in the majority of practical vibration scenarios. In recent studies, some researchers have proposed 2DOF

energy harvester models to achieve two closer resonant frequencies. Figs. 1c and 1d show a 2DOF PEH model (Tang and Yang, 2012) and a 2DOF EMEH model, respectively. In Figs. 1c and 1d, a 2DOF PEH model and a 2DOF EMEH model have the same mechanical subsystems and different electrical subsystems for power generation. For the mechanical subsystem of these two models, a mass M_1 with spring K_1 and damping C_1 is connected to the base, and the mass M_2 with spring K_2 and damping C_2 is connected to the mass M_1. For the electrical subsystem of the 2DOF PEH model, a piezoelectric transducer for voltage generation is placed between the mass M_1 and the base (Fig. 1c). For the electrical subsystem of the 2DOF EMEH model, a coil for the current generation is placed in the axis of the motion of the magnet mass M_2 (Fig. 1d).

The mass M_2 of the 2DOF PEH model (Fig. 1c) or the mass M_1 of the 2DOF EMEH model (Fig. 1d) is only used to achieve two close resonant frequencies and thus a wider operating bandwidth compared to 1DOF harvester. Actually, they can be further exploited to convert mechanical energy into electrical energy using an additional transducer. We propose a 2DOF hybrid P-EMEH model (Fig. 1e). As the base vibrates, the piezoelectric transducer placed between the base and the mass M_1 is deformed to generate the voltage across the resistor R_{L1} by the piezoelectric effect. At the same time, the magnetic mass M_2 moves in and out of the coil and the coil generates induced current flowing through the resistor R_{L2} according to Faraday's law. In Fig. 1, u_0, u_1, and u_2 are the absolute coordinates of the base, M_1, and M_2, respectively. With this design, we aim at exploiting the full potential of the additional mechanical subsystem in a conventional 2DOF energy harvester model.

3 Analytical modelling of 2DOF hybrid P-EMEH

In Fig. 1e, setting $r_1=u_1-u_0$ and $r_2=u_2-u_1$, the mechanical governing equation of the 2DOF hybrid P-EMEH system can be written as

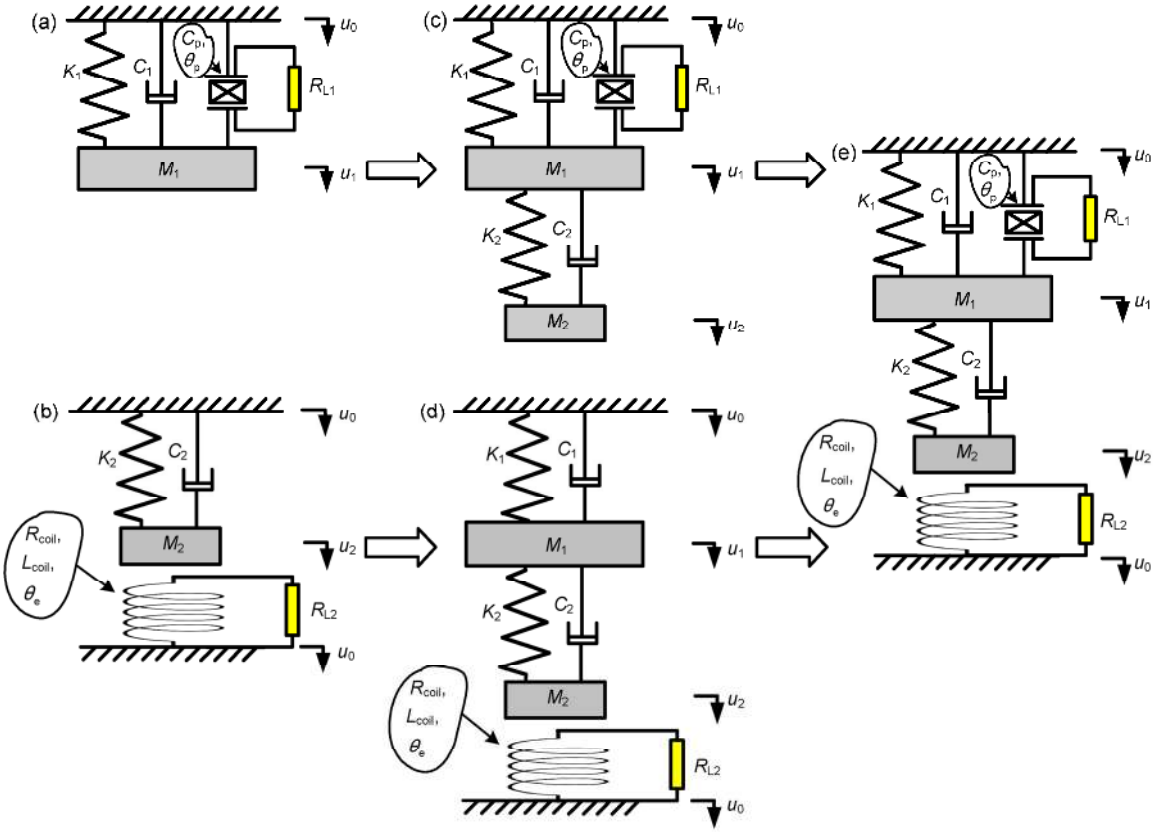

Fig. 1 Various energy harvester models: (a) 1DOF PEH; (b) 1DOF EMEH; (c) 2DOF PEH (Tang and Yang, 2012); (d) 2DOF EMEH; (e) 2DOF hybrid P-EMEH

$$\begin{cases}(M_1+M_2)\ddot{r}_1+C_1\dot{r}_1+K_1r_1+M_2\ddot{r}_2+F_\mathrm{p}+F_\mathrm{e}\\ \qquad\qquad =-(M_1+M_2)\ddot{u}_0,\\ M_2\ddot{r}_2+C_2\dot{r}_2+K_2r_2+F_\mathrm{e}=-M_2\ddot{r}_1-M_2\ddot{u}_0,\end{cases}\tag{1}$$

where K_1 and K_2 are the spring stiffness of mass M_1 and M_2, respectively. C_1 and C_2 are the mechanical damping of mass M_1 and M_2, respectively. As the 2DOF hybrid P-EMEH delivers energy to the load resistances, the mechanical domain receives the feedback from the electrical domain, which is represented by the backward electromechanical coupling forces, F_p and F_e. F_p is the backward coupling force due to the creation of the voltage across the piezoelectric element, which is given by

$$F_\mathrm{p}=\theta_\mathrm{p}V_\mathrm{R1},\tag{2}$$

where V_R1 is the voltage across the resistor R_L1, and θ_p is the piezoelectric coupling coefficient. F_e is the backward coupling force due to the creation of an opposing magnetic field by the current flowing through the coil, which is given by

$$F_\mathrm{e}=\theta_\mathrm{e}I_\mathrm{R2},\tag{3}$$

where I_R2 is the current flowing through the resistor R_L2, and θ_e is the electromagnetic coupling coefficient, $\theta_\mathrm{e}=B_1l$, where B_1 and l are the average magnetic flux density and the total length of the coil, respectively.

The simplified electrical models of the piezoelectric and electromagnetic transducers are given in Fig. 2a and Fig. 2b, respectively. In Fig. 2a, the electrical model of the piezoelectric transducer consists of a current source I_p in parallel with its internal capacitance C_p, where the output terminal is connected with the resistor R_L1. In Fig. 2b, the electrical model of the electromagnetic transducer consists of a voltage source V_e in series with its internal inductance L_coil and the coil resistance R_coil, where the output terminal is connected with the resistor R_L2.

According to Kirchhoff's current law, the circuit-governing equation for piezoelectric transduction of the system (Fig. 2a) is written as

$$-I_\mathrm{p}+C_\mathrm{p}\dot{V}_\mathrm{R1}+\frac{V_\mathrm{R1}}{R_\mathrm{L1}}=0,\tag{4}$$

where the current I_p is proportional to the velocity $\dot{r}_1$ in the mechanical domain, i.e., $I_\mathrm{p}=\theta_\mathrm{p}\dot{r}_1$.

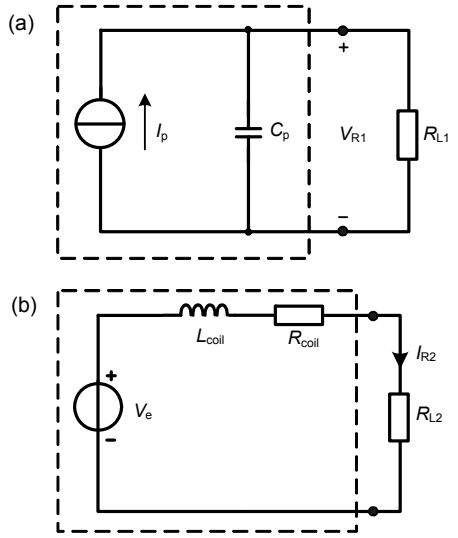

Fig. 2 Equivalent electrical models of piezoelectric transducer (a) and electromagnetic transducer (b)

According to Kirchhoff's voltage law, the circuit-governing equation for electromagnetic transduction of the system (Fig. 2b) is written as

$$-V_\mathrm{e}+L_\mathrm{coil}\dot{I}_\mathrm{R2}+(R_\mathrm{coil}+R_\mathrm{L2})I_\mathrm{R2}=0,\tag{5}$$

where the voltage V_e is proportional to the velocity $(\dot{r}_1+\dot{r}_2)$ in the mechanical domain, i.e., $V_\mathrm{e}=\theta_\mathrm{e}(\dot{r}_1+\dot{r}_2)$.

Substituting Eqs. (2) and (3) into Eq. (1) and further combining Eqs. (1), (4), and (5), the electromechanical model of the 2DOF hybrid P-EMEH is written as

$$\begin{cases}(M_1+M_2)\ddot{r}_1+C_1\dot{r}_1+K_1r_1+M_2\ddot{r}_2+\theta_\mathrm{p}V_\mathrm{R1}+\theta_\mathrm{e}I_\mathrm{R2}\\ \qquad\qquad =-(M_1+M_2)\ddot{u}_0,\\ M_2\ddot{r}_2+C_2\dot{r}_2+K_2r_2+\theta_\mathrm{e}I_\mathrm{R2}=-M_2\ddot{r}_1-M_2\ddot{u}_0,\\ -\theta_\mathrm{p}\dot{r}_1+C_\mathrm{p}\dot{V}_\mathrm{R1}+V_\mathrm{R1}/R_\mathrm{L1}=0,\\ -\theta_\mathrm{e}(\dot{r}_1+\dot{r}_2)+L_\mathrm{coil}\dot{I}_\mathrm{R2}+(R_\mathrm{coil}+R_\mathrm{L2})I_\mathrm{R2}=0.\end{cases}\tag{6}$$

Letting $\omega_1=\sqrt{K_1/M_1}$, $\omega_2=\sqrt{K_2/M_2}$, $\zeta_1=C_1/(2M_1\omega_1)$, $\zeta_2=C_2/(2M_2\omega_2)$, and $u=M_2/M_1$, and applying the Laplace transform for Eq. (6), we can obtain:

$$\begin{cases}[(1+u)s^2+2\zeta_1\omega_1 s+\omega_1^2]\hat{r}_1+us^2\hat{r}_2+(\theta_p/M_1)V_{R1}\\ \qquad +(\theta_e/M_1)\hat{I}_{R2}=-(1+u)s^2\hat{u}_0,\\ (s^2+2\zeta_2\omega_2 s+\omega_2^2)\hat{r}_2+\left(\dfrac{\theta_e}{uM_1}\right)\hat{I}_{R2}=-s^2\hat{r}_1-s^2\hat{u}_0,\\ -\theta_p s\hat{r}_1+C_p s\hat{V}_{R1}+\hat{V}_{R1}/R_{L1}=0,\\ -\theta_e s(\hat{r}_1+\hat{r}_2)+L_{coil}s\hat{I}_{R2}+(R_{coil}+R_{L2})\hat{I}_{R2}=0,\end{cases} \quad (7)$$

where s is the Laplace variable, ω_1 and ω_2 are the natural angular frequencies when the two subsystems work separately.

Solving Eq. (7) and letting s=jω, the voltage across the resistor R_{L1} is obtained as

$$\left|\frac{\hat{V}_{R1}}{\omega^2\hat{u}_0}\right|=\frac{M_1}{|\theta_p|}\left|\left(1+\frac{u(\alpha^2+\mathrm{j}2\zeta_2\alpha\Omega_1)}{A}\right)\right.$$
$$\left.\Big/\left(\left(1-\Omega_1^2+\mathrm{j}2\zeta_1\Omega_1+u(\alpha^2+\mathrm{j}2\zeta_2\alpha\Omega_1)\right.\right.\right. \quad (8)$$
$$\left.\left.\left.-u(\alpha^2+\mathrm{j}2\zeta_2\alpha\Omega_1)^2/A\right)\frac{\mathrm{j}\omega_p\Omega_1+1}{\mathrm{j}k_p^2\omega_p\Omega_1}+1\right)\right|,$$

and the current through the resistor R_{L2} is obtained as

$$\left|\frac{\hat{I}_{R2}}{\omega^2\hat{u}_0}\right|=\frac{uM_1}{|\theta_e|}\left|\left(1+\frac{\alpha^2+\mathrm{j}2\zeta_2\alpha\Omega_1}{B}\right)\right.$$
$$\left.\Big/\left(\left(\alpha^2-\Omega_1^2+\mathrm{j}2\zeta_2\alpha\Omega_1-u(\alpha^2+\mathrm{j}2\zeta_2\alpha\Omega_1)^2/B\right)\right.\right. \quad (9)$$
$$\left.\left.\times\frac{\mathrm{j}\Omega_1+\alpha\omega_e}{\mathrm{j}k_e^2\alpha^2\Omega_1}+1\right)\right|,$$

where j is the imaginary unit, ω is the excitation angular frequency, and the dimensionless parameters are

$$\alpha=\frac{\omega_2}{\omega_1},\ \Omega_1=\frac{\omega}{\omega_1},\ k_p^2=\frac{\theta_p^2}{C_pK_1},\ \omega_p=R_{L1}C_p\omega_1,$$
$$k_e^2=\frac{\theta_e^2}{L_{coil}K_2},\ \omega_e=\frac{R_{coil}+R_{L2}}{\omega_2L_{coil}},$$
$$A=\alpha^2-\Omega_1^2+\mathrm{j}2\zeta_2\alpha\Omega_1+\frac{\mathrm{j}k_e^2\alpha^2\Omega_1}{\mathrm{j}\Omega_1+\alpha\omega_e},$$
$$B=1-\Omega_1^2+\mathrm{j}2\zeta_1\Omega_1+u(\alpha^2+\mathrm{j}2\zeta_2\alpha\Omega_1)+\frac{\mathrm{j}k_p^2\omega_p\Omega_1}{\mathrm{j}\omega_p\Omega_1+1}.$$

The power outputs on the resistors R_{L1} and R_{L2} are then obtained as

$$\left|\frac{\hat{P}_{R1}}{(\omega^2\hat{u}_0)^2}\right|=\frac{M_1}{\omega_1\omega_pk_p^2}\left|\left(1+\frac{u(\alpha^2+\mathrm{j}2\zeta_2\alpha\Omega_1)}{A}\right)\right.$$
$$\left.\Big/\left(\left(1-\Omega_1^2+\mathrm{j}2\zeta_1\Omega_1+u(\alpha^2+\mathrm{j}2\zeta_2\alpha\Omega_1)\right.\right.\right. \quad (10)$$
$$\left.\left.\left.-u(\alpha^2+\mathrm{j}2\zeta_2\alpha\Omega_1)^2/A\right)\frac{\mathrm{j}\omega_p\Omega_1+1}{\mathrm{j}k_p^2\omega_p\Omega_1}+1\right)\right|^2,$$

$$\left|\frac{\hat{P}_{R2}}{(\omega^2\hat{u}_0)^2}\right|=\frac{uM_1\omega_e}{\alpha\omega_1k_e^2(1+R_{coil}/R_{L2})}$$
$$\times\left|\left(1+\frac{\alpha^2+\mathrm{j}2\zeta_2\alpha\Omega_1}{B}\right)\right/\left(\left(\alpha^2-\Omega_1^2+\mathrm{j}2\zeta_2\alpha\Omega_1\right.\right. \quad (11)$$
$$\left.\left.-u(\alpha^2+\mathrm{j}2\zeta_2\alpha\Omega_1)^2/B\right)\frac{\mathrm{j}\Omega_1+\alpha\omega_e}{\mathrm{j}k_e^2\alpha^2\Omega_1}+1\right)\right|^2.$$

The total power of the 2DOF hybrid P-EMEH energy harvester is

$$\hat{P}_{total}=\hat{P}_{R1}+\hat{P}_{R2}. \quad (12)$$

As $R_{L2}\to\infty$, $\omega_e\to\infty$, and $A\to\alpha^2-\Omega_1^2+\mathrm{j}2\zeta_2\alpha\Omega_1$, Eq. (12) is reduced to $\hat{P}_{total}\to\hat{P}_{R1}$, and Eq. (10) is reduced to

$$\left|\frac{\hat{P}_{R1}}{(\omega^2\hat{u}_0)^2}\right|\to\frac{M_1}{\omega_1\omega_pk_p^2}\left|\left(1+u+\frac{u\Omega_1^2}{\alpha^2-\Omega_1^2+\mathrm{j}2\zeta_2\alpha\Omega_1}\right)\right.$$
$$\left.\Big/\left[\left(1-(1+u)\Omega_1^2+\mathrm{j}2\zeta_1\Omega_1\right.\right.\right. \quad (13)$$
$$\left.\left.\left.-\frac{u\Omega_1^4}{\alpha^2-\Omega_1^2+\mathrm{j}2\zeta_2\alpha\Omega_1}\right)\frac{\mathrm{j}\omega_p\Omega_1+1}{\mathrm{j}k_p^2\omega_p\Omega_1}+1\right]\right|^2,$$

which is the power output of the conventional 2DOF PEH (Fig. 1c). Furthermore, as $M_2\to0$, the mass ratio $u\to0$ and Eq. (13) is reduced to

$$\left|\frac{\hat{P}_{R1}}{(\omega^2\hat{u}_0)^2}\right|\to\frac{M_1}{\omega_1\omega_pk_p^2}$$
$$\times\left|1\Big/\left((1-\Omega_1^2+\mathrm{j}2\zeta_1\Omega_1)\frac{\mathrm{j}\omega_p\Omega_1+1}{\mathrm{j}k_p^2\omega_p\Omega_1}+1\right)\right|^2, \quad (14)$$

which is the power output of the conventional 1DOF PEH (Fig. 1a).

As $R_{L1}\to 0$, $\omega_p\to 0$, and $B\to 1-\Omega_1^2+j2\zeta_1\Omega_1+u(\alpha^2+j2\zeta_2\alpha\Omega_1)$, Eq. (12) is reduced to $\hat{P}_{total}\to\hat{P}_{R2}$, and Eq. (11) is reduced to

$$\left|\frac{\hat{P}_{R2}}{(\omega^2\hat{u}_0)^2}\right|\to\frac{uM_1\omega_e}{\alpha\omega_1k_e^2(1+R_{coil}/R_{L2})}\times\left|\left(1+\frac{\alpha^2+j2\zeta_2\alpha\Omega_1}{1-\Omega_1^2+j2\zeta_1\Omega_1+u(\alpha^2+j2\zeta_2\alpha\Omega_1)}\right)\Big/\left[\left(\alpha^2-\Omega_1^2+j2\zeta_2\alpha\Omega_1-u(\alpha^2+j2\zeta_2\alpha\Omega_1)^2\Big/\left(1-\Omega_1^2+j2\zeta_1\Omega_1+u(\alpha^2+j2\zeta_2\alpha\Omega_1)\right)\right)\times\frac{j\Omega_1+\alpha\omega_e}{jk_e^2\alpha^2\Omega_1}+1\right]\right|^2, \quad (15)$$

which is the power output of the conventional 2DOF EMEH (Fig. 1d).

In Eq. (15), letting $\Omega_1=\alpha\Omega_2$, $M_1=M_2/u$ and $\omega_1=\omega_2/\alpha$. As $K_1\to\infty$, the frequency ratio $\alpha\to 0$ and Eq. (15) is reduced to

$$\left|\frac{\hat{P}_{R2}}{(\omega^2\hat{u}_0)^2}\right|\to\frac{M_2\Omega_2^2k_e^2\omega_e}{\omega_2(1+R_{coil}/R_{L2})}\times\left|\frac{1}{(1-\Omega_2^2+j2\zeta_2\Omega_2)(j\Omega_2+\omega_e)+jk_e^2\Omega_2}\right|^2, \quad (16)$$

which is the power output of the conventional 1DOF EMEH (Fig. 1b).

4 Experimental validation

4.1 Experimental setup

Fig. 3 shows the prototype of the proposed 2DOF hybrid P-EMEH. It can be seen that the PEH part is a clamped-clamped piezoelectric beam with a central mass and two piezoelectric elements bonded symmetrically on the brass beam. The two piezoelectric elements are electrically connected in parallel. The EMEH part consists of a spring, a magnet, and a wound coil. One end of the spring is connected with the central mass of the PEH part and the other with the magnet. A copper wound coil is placed on the base, the axis of which aligns with the direction of the motion of the magnet. The material and geometric parameters of the PEH, magnet, and coil are given in Tables 1 and 2, respectively.

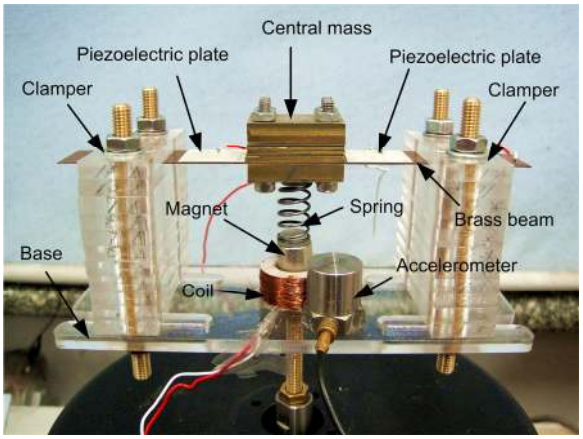

Fig. 3 Experimental prototype of 2DOF hybrid P-EMEH

Table 1 Parameters of PEH part

Parameter	Value
Clamped length of the brass beam (mm)	80
Width of the brass beam (mm)	20
Thickness of the brass beam (mm)	0.5
Thickness of the piezoelectric element (mm)	0.2
Static clamped capacitance, C_p (nF)	42
Effective mass of the beam with central mass, M_1 (g)	104
Damping ratio of PEH, ζ_1	0.014

Table 2 Parameters of magnet and coil

Parameter	Value
Effective mass of the spring and the magnet, M_2 (g)	10
Mass of the coil part (g)	16
Radius of the magnet, r_m (mm)	6
Height of the magnet, h_m (mm)	10
Residual the flux density, B_r (T)	1.1
Nearest distance between the coil and Magnet, z_1 (mm)	2.8
Height of the wounded coil (mm)	15
Total length of the coil, l (m)	52.15
Inductance of the coil, L_{coil} (mH)	40.6
Resistance of the coil, R_{coil} (Ω)	116
Damping ratio of EMEH, ζ_2	0.0035

It should be mentioned that if the coil is open-circuited, there is no power output from the EMEH part and the electromagnetic backward coupling force disappears. Thus, the system behaves as a 2DOF PEH. If the piezoelectric elements are short-circuited, there is no power output from the PEH part and the piezoelectric backward coupling force disappears. Thus, the energy harvesting system behaves as a 2DOF EMEH. If the spring is detached from the central mass, the system degrades to a 1DOF PEH. If we replace the current brass beam with a much thicker and thus much stiffer one, the relative displacement between the central mass and the base can be neglected and the EMEH part can be regarded as a 1DOF EMEH subjected to the base excitation. We will compare the performances of these five configurations in the experiment and validate the derived theoretical models later.

Fig. 4 shows the experimental setup. The prototype 2DOF hybrid P-EMEH is mounted on an electrodynamic shaker. An accelerometer is mounted on the platform of the harvester to measure the base excitations. The shaker is connected to a signal generator through a power amplifier. The signal generator and power amplifier are tuned manually to provide the desired excitation to the system. The output terminals of the piezoelectric elements and the wound coil are connected to two respective variable resistors. The power outputs from the PEH part and the EMEH part are added at each frequency and we searched for the optimal total power by altering the two resistors.

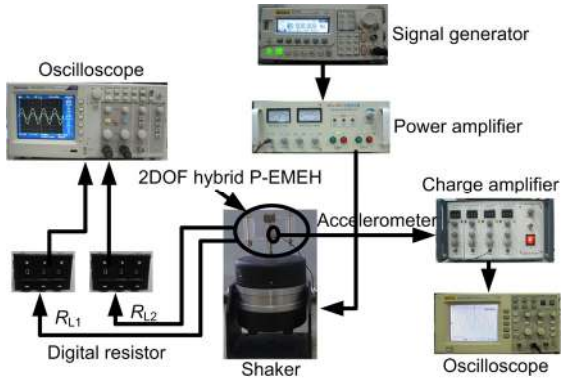

Fig. 4 Experiment setup of 2DOF hybrid P-EMEH

Prior to the model validation, the system parameters should be determined. The average magnetic flux density of the cylindrical magnet, B_1, is approximated by considering the coil divided into n sections,

$$B_1=\frac{B_r}{2}\frac{1}{n}\sum_{i=1}^{n}\left[\frac{z_i+h_m}{\sqrt{(z_i+h_m)^2+r_m^2}}-\frac{z_i}{\sqrt{z_i^2+r_m^2}}\right], \quad (17)$$

where z_i is the distance from the magnet to the ith cross section of the coil. Between the nearest distance from the magnet z_1=2.8 mm and the farthest distance z_n=17.8 mm, we consider increments of 0.1 mm and thus n=151. According to Eq. (17), the average magnetic flux density B_1=0.0789 T.

Other parameters can be determined from the experiment. Due to the piezoelectric coupling, 1DOF PEH (removing the spring and magnet) possesses a short circuit resonant frequency f_{sc} (when the load resistance approaches 0) and an open circuit resonant frequency f_{oc} (when the load resistance approaches infinity). In this study, we use two different resistors (R_{L1}=100 Ω and R_{L1}=1 MΩ) to obtain the voltage frequency responses of 1DOF PEH, which approximate the short circuit and open circuit conditions, respectively. According to these responses, f_{sc} and f_{oc} are measured as 81.5 Hz and 81.8 Hz, respectively. The EMCC of the 1DOF PEH can be calculated as 0.086 according to the equation $k_p=[(\omega_{oc}/\omega_{sc})^2-1]^{1/2}$, where ω_{sc} and ω_{oc} are the short circuit and open circuit resonant angular frequencies, respectively. $\omega_{sc}=2\pi f_{sc}$ and $\omega_{oc}=2\pi f_{oc}$. Note that in Eq. (7), ω_1 refers to the natural angular frequency of the mechanical structure for the 1DOF PEH without considering the backward piezoelectric coupling effect, i.e., the piezoelectric element approximates the short circuit. Thus, $\omega_1=\omega_{sc}$=512.08 rad/s. Similarly, ω_2 refers to the natural angular frequency of the mechanical structure for 1DOF EMEH (the spring with the magnetic element only) without considering the backward electromagnetic coupling effect, i.e., the coil is open circuit. According to the voltage frequency response, the open circuit resonance frequency f_2 is measured as 76 Hz, and thus, $\omega_2=2\pi f_2$=477.52 rad/s. Furthermore, the frequency ratio $\alpha=\omega_2/\omega_1$=0.9325. The EMCC of the 1DOF EMEH can be calculated as 0.4277 according to the equation $k_e=\theta_e/(L_{coil}K_2)^{1/2}$, where $K_2=M_2\omega_2^2$. The damping ratios ζ_1 and ζ_2 of the 1DOF PEH and 1DOF EMEH, which are also the damping ratios of the PEH

part and EMEH part in the 2DOF hybrid P-EMEH, can be determined by the log decrement method from the voltage attenuation curves of the PEH and EMEH, respectively.

$$\zeta = \frac{1}{2\pi k}\ln\left(\frac{A_1}{A_{k+1}}\right), \tag{18}$$

where A_1 is the first amplitude of the attenuation curve, and k is the decaying cycle. The damping ratios of ζ_1 and ζ_2 are given in Tables 1 and 2, respectively.

4.2 Results

Figs. 5a and 5b show the experimental and simulation results from various harvester configurations, respectively. The experiment and simulation are both conducted under an excitation level of 1 m/s^2 (root mean square value). Note that the 1DOF PEH has a sole peak of 0.69 mW and the 1DOF EMEH has a sole peak of 0.48 mW in the frequency range of 65 Hz–95 Hz. The 2DOF energy harvester prototypes (2DOF PEH, 2DOF EMEH, and the proposed 2DOF hybrid P-EMEH) can achieve two peaks in this frequency range, providing wider operating bandwidth. To further compare the maximum power outputs of the five harvester configurations, they are divided into two groups. One group includes 1DOF PEH, 2DOF PEH, and 2DOF hybrid P-EMEH, and the other group includes 1DOF EMEH, 2DOF EMEH, and 2DOF hybrid P-EMEH. Note that in Fig. 5a, the 2DOF hybrid P-EMEH has improved the maximum power output (2.16 mW) as compared to the 2DOF PEH (0.96 mW) and 1DOF PEH (0.69 mW). Similarly, the 2DOF hybrid P-EMEH also provides a better performance than the 2DOF EMEH (1.68 mW) and 1DOF EMEH (0.48 mW). In addition, note that the second mode of the 2DOF hybrid P-EMEH provides comparable output as 1DOF PEH and 1DOF EMEH. Furthermore, it is worth mentioning that the 2DOF hybrid P-EMEH has improved the maximum power density (16.6 mW/kg) as compared to the other 2DOF configurations (2DOF PEH, 8.4 mW/kg; 2DOF EMEH, 12.9 mW/kg) and the 1DOF PEH (6.6 mW/kg). Though it is slightly lower than that of the 1DOF EMEH (18.5 mW/kg), the much enhanced maximal power output (2.16 mW) achieved and two close resonant modes (for wider bandwidth) of the 2DOF hybrid P-EMEH as compared to the 1DOF EMEH are worth this slight sacrifice in power density.

Fig. 5b shows the analytical solution with the system parameters determined from experiment (Tables 1 and 2). Note that in Fig. 5b, the predicted maximum power outputs for various harvester configurations and the overall trends of the analytical prediction are quite consistent with the experiment results (Fig. 5a).

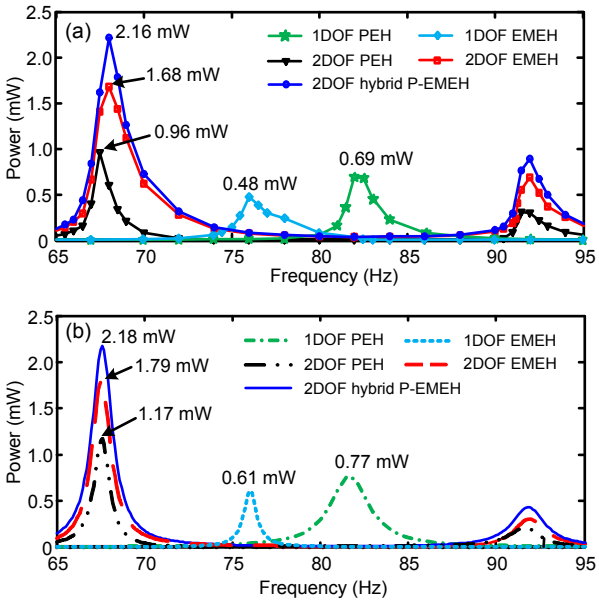

Fig. 5 Power outputs from various configurations for k_p=0.086 and k_e=0.4277: (a) experiment and (b) simulation

Both experimental and simulation results indicate that with current system parameters (e.g., coupling coefficients), the hybrid scheme can provide advantageous performance over the stand-alone piezoelectric or electromagnetic techniques.

5 Effects of electromechanical coupling

With the validated 2DOF hybrid P-EMEH model, we further study the effects of the EMCC on the maximum power outputs. First, we investigate how the EMCC affects the overall performance and how the two conversion mechanisms affect each other in a 2DOF hybrid P-EMEH model. Subsequently, we compare the effect of the EMCC on power outputs of various harvester configurations including 1DOF

PEH, 2DOF PEH, 1DOF EMEH, 2DOF EMEH, and 2DOF hybrid P-EMEH models.

Figs. 6a and 6b show the maximum power outputs from piezoelectric and electromagnetic transducers used in a 2DOF hybrid P-EMEH against two effective EMCCs k_p and k_e, respectively. In Fig. 6a, the electromagnetic coupling k_e is fixed (k_e=0.4277) and the piezoelectric coupling k_p increases. Before the saturation of power output, an increase of k_p leads to an increase in piezoelectric and total power outputs, and a decrease in electromagnetic power output. Similarly, in Fig. 6b, k_p is fixed (k_p=0.086) and the electromagnetic coupling k_e increases. Before the saturation of power output, an increase of k_e leads to an increase in electromagnetic and total power outputs, and a decrease in piezoelectric power output. These results indicate that when piezoelectric and electromagnetic transducers exist in an energy harvesting device, they interact in an opposite way, i.e., the increase of the power output from one electromechanical transducer by increasing its coupling will lead to the decrease of the power output from the other. The main reason is that for a 2DOF hybrid P-EMEH system, both piezoelectric and electromagnetic coupling will induce electrical damping and suppress the vibrations of the system. In Fig. 6a, as k_p increases, more energy is converted into electricity via the PEH part and so induces more damping and thus suppresses the vibrations of the system. Since k_e is fixed, the suppressed vibrations result in less contribution of power output from EMEH part. Similarly, in Fig. 6b, as k_e increases, more energy is harnessed via the EMEH part and so induces more damping to the system. Since k_p is fixed, the suppressed vibrations result in the decrease of power output from the PEH part.

Figs. 7a and 7b show the maximum power outputs from various harvester configurations against two effective EMCCs k_p and k_e, respectively. It can be seen from Fig. 7a that an increase of k_p leads to an increase in power outputs in the 1DOF PEH, 2DOF PEH, and 2DOF hybrid P-EMEH models first, but finally the power outputs reach saturation in each case. The trends of power versus coupling from these energy harvesters are the same as the 1DOF PEH in previous studies (Guyomar *et al.*, 2005; Liao and Sodano, 2008). Similarly, in Fig. 7b, an increase of k_e

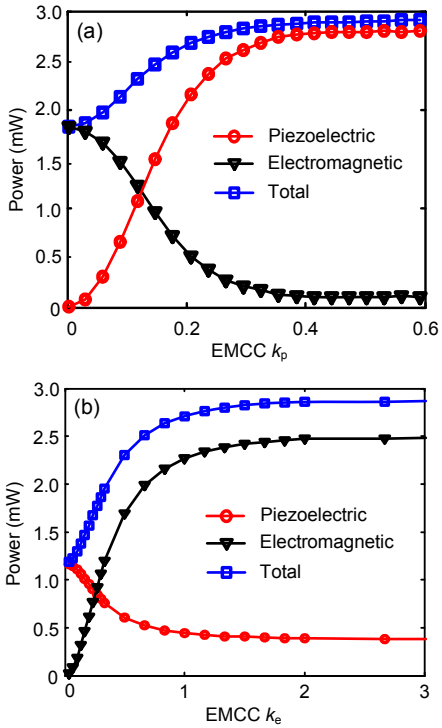

Fig. 6 Maximum power outputs from 2DOF hybrid P-EMEH versus piezoelectric EMCC k_p (k_e=0.4277) (a) and electromagnetic EMCC k_e (k_p=0.086) (b)

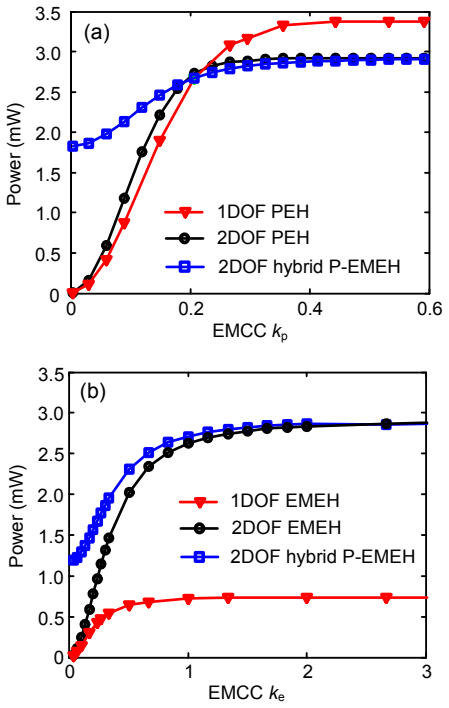

Fig. 7 Maximum power outputs from various harvester configurations versus piezoelectric EMCC k_p (k_e=0.4277) (a) and electromagnetic EMCC k_e (k_p=0.086) (b)

leads to an increase in power outputs from the 1DOF EMEH, 2DOF EMEH, and 2DOF hybrid P-EMEH models first, but finally the power outputs reach saturation in each case. The trends of power versus coupling are similar to the 1DOF EMEH in previous study (Challa *et al*., 2013). Moreover, both 2DOF EMEH and 2DOF hybrid P-EMEH have significantly improved power outputs as compared to the 1DOF EMEH.

To investigate the performance of the energy harvesters in different coupling regions, some researchers (Shu and Lien, 2006) proposed using the parameter $\gamma_1=k_p^2/\zeta_1$ as an indicator of the piezoelectric coupling strength of 1DOF PEH and proposed the criterion of strong coupling, i.e., $k_p^2/\zeta_1\geq 4(\zeta_1+1)$ for an AC interface circuit (pure resistor). Applying this criterion and considering $\zeta_1=0.014$ in this work, we have $k_p\geq 0.238$ for the strong coupling of 1DOF PEH. For $k_p=0.238$, the power output corresponds to 90% of the saturation power output. Similarly, some researchers (Challa *et al.*, 2013) proposed using the parameter $\gamma_2=\theta_e^2/(R_{coil}C_2)$ to indicate the coupling strength of the 1DOF EMEH and studied the power outputs when loosely coupled ($\gamma_2 \ll 1$), critically coupled ($\gamma_2=1$), and strongly coupled ($\gamma_2 \gg 1$). The equation can also be written as $\gamma_2=L_{coil}\omega_2 k_e^2/(2R_{coil}\zeta_2)$, where $k_e^2=\theta_e^2/(L_{coil}K_2)$, $\zeta_2=C_2/(2M_2\omega_2)$, and $\omega_2=(K_2/M_2)^{1/2}$. Challa *et al.* (2013) did not clearly provide the criterion for quantitatively defining the boundaries of coupling strength. We apply a similar criterion as 1DOF PEH, i.e., 90% of saturation power output, to define the strong coupling of 1DOF EMEH. We obtained the critical value of $k_e=0.66$ with the system parameters in our work. Considering $L_{coil}=40.6$ mH, $R_{coil}=116\ \Omega$, $\zeta_2=0.0035$, and $\omega_2=477.52$ rad/s in our work, $\gamma_2=10.4$. The result is consistent with the condition of a strongly coupled system ($\gamma_2 \gg 1$) in (Challa *et al*., 2013). This implies that 90% of saturation power output can be used to define the strong coupling of 1DOF PEH and 1DOF EMEH. In addition, to our best knowledge, there is no literature discussing the effect of coupling on the performance of a 2DOF harvester system, no matter whether it is purely piezoelectric, electromagnetic, or hybrid. We apply 90% of saturation power output to define strong coupling for 2DOF hybrid P-EMEH. For the 2DOF hybrid system, due to the opposite interaction between the two electromechanical couplings, we can only determine the critical value of k_p for strong coupling when k_e is given, and vice versa. In Fig. 7a, given $k_e=0.4277$, 90% of saturation power output requires $k_p=0.2$. Hence, $0<k_p<0.2$ is regarded as the weak and medium coupling range. Given k_p in the range of 0–0.2, the 2DOF hybrid P-EMEH has an improved power output as compared to the 1DOF PEH and 2DOF PEH. Beyond the critical value of $k_p=0.2$, both 2DOF PEH and 2DOF hybrid P-EMEH are near the saturation of power, and the power output of the 2DOF hybrid P-EMEH has no advantage over the 2DOF PEH and is even smaller than that of the 1DOF PEH. Similarly, in Fig. 7b, given $k_p=0.086$, 90% of saturation power output requires $k_e=0.9$. Hence, $0<k_e<0.9$ is regarded as the weak and medium coupling range. Given k_e in the range of 0–0.9, the 2DOF hybrid P-EMEH provides better performance than the 2DOF EMEH and 1DOF EMEH. These results suggest that the hybrid energy harvester configuration is advantageous over the stand-alone harvester configurations in both weak and medium coupling regimes.

6 Conclusions

This paper presents a 2DOF hybrid P-EMEH design combing piezoelectric and electromagnetic transduction mechanisms. The mathematical model of the 2DOF hybrid P-EMEH is established and validated experimentally. The prototype 2DOF hybrid P-EMEH demonstrates its advantageous performance in terms of both wider bandwidth and improved power magnitude as compared to the conventional 1DOF and 2DOF harvester configurations with stand-alone conversion mechanisms. With the validated mathematical model, the effect of the piezoelectric and electromagnetic coupling coefficients on the performances of various harvester configurations is analyzed. For the 2DOF hybrid P-EMEH model, although the increase of the power output from one electromechanical transducer will lead to the decrease of the power output from the other, the total power output of the 2DOF hybrid P-EMEH model increases before it reaches its saturation. In the weak and medium coupling scenarios, the hybrid 2DOF energy harvester configuration provides an efficient way to enhance device performance.

References

Aldraihem, O., Baz, A., 2011. Energy harvester with dynamic magnifier. *Journal of Intelligent Material Systems and Structures*, **22**(6):521-530. [doi:10.1177/1045389X11402706]

Arafa, M., Akl, W., Aladwani, A., *et al*., 2011. Experimental implementation of a cantilevered piezoelectric energy harvester with a dynamic magnifier. Proceedings of SPIE, Active and Passive Smart Structures and Integrated Systems, San Diego, USA, p.79770Q. [doi:10.1117/12.880689]

Challa, V.R., Prasad, M.G., Fisher, F.T., 2009. Coupled piezoelectric-electromagnetic energy harvesting technique for achieving increased power output through damping matching. *Smart Materials and Structures*, **18**(9):095029. [doi:10.1088/0964-1726/18/9/095029]

Challa, V.R., Cheng, S., Arnold, D.P., 2013. The role of coupling strength in the performance of electrodynamic vibrational energy harvesters. *Smart Materials and Structures*, **22**(2):025005. [doi:10.1088/0964-1726/22/2/025005]

Dutoit, N.E., Wardle, B.L., Kim, S.G., 2005. Design considerations for MEMS-scale piezoelectric mechanical vibration energy harvesters. *Integrated Ferroelectrics*, **71**(1):121-160. [doi:10.1080/10584580590964574]

Elvin, N.G., Elvin, A.A., 2011. An experimentally validated electromagnetic energy harvester. *Journal of Sound and Vibration*, **330**(10):2314-2324. [doi:10.1016/j.jsv.2010.11.024]

Guyomar, D., Badel, A., Lefeuvre, E., *et al*., 2005. Toward energy harvesting using active materials and conversion improvement by nonlinear processing. *IEEE Transctions on Ultrasonics, Ferroelectrics, and Frequency Control*, **52**(4):584-595. [doi:10.1109/TUFFC.2005.1428041]

Harne, R.L., 2012. Theoretical investigations of energy harvesting efficiency from structural vibrations using piezoelectric and electromagnetic oscillators. *The Journal of the Acoustical Society of America*, **132**(1):162-172. [doi:10.1121/1.4725765]

Jung, H.J., Kim, I.H., Koo, J.H., 2011. A multi-functional cable-damper system for vibration mitigation, tension estimation and energy harvesting. *Smart Structures and Systems*, **7**(5):379-392. [doi:10.12989/sss.2011.7.5.379]

Khaligh, A., Zeng, P., Wu, X., *et al*., 2008. A hybrid energy scavenging topology for human-powered mobile electronics. Proceedings-34th Annual Conference of the IEEE Industrial Electronics Society, Orlando, USA, p.448-453. [doi:10.1109/IECON.2008.4757995]

Kim, H., Kim, S.M., Son, H., *et al*., 2012. Enhancement of piezoelectricity via electrostatic effects on a textile platform. *Energy & Environmental Science*, **5**(10):8932-8936. [doi:10.1039/c2ee22744d]

Lallart, M., Pruvost, S., Guyomar, D., 2011. Electrostatic energy harvesting enhancement using variable equivalent permittivity. *Physics Letters A*, **375**(45):3921-3924. [doi:10.1016/j.physleta.2011.09.043]

Liao, Y.B., Sodano, H.A., 2008. Model of a single mode energy harvester and properties for optimal power generation. *Smart Materials and Structures*, **17**(6):065026. [doi:10.1088/0964-1726/17/6/065026]

Lumentut, M.F., Howard, I.M., 2011. Analytical modeling of self-powered electromechanical piezoelectric bimorph beams with multidirectional excitation. *International Journal of Smart and Nano Materials*, **2**(3):134-175. [doi:10.1080/19475411.2011.592868]

Roundy, S., Wright, P.K., Rabaey, J., 2003. A study of low level vibrations as a power source for wireless sensor nodes. *Computer Communications*, **26**(11):1131-1144. [doi:10.1016/S0140-3664(02)00248-7]

Shan, X.B., Guan, S.W., Liu, Z.S., *et al*., 2013. A new energy harvester using a piezoelectric and suspension electromagnetic mechanism. *Journal of Zhejiang University-SCIENCE A (Applying Physics & Engineering)*, **14**(12):890-897. [doi:10.1631/jzus.A1300210]

Shu, Y.C., Lien, I.C., 2006. Analysis of power output for piezoelectric energy harvesting systems. *Smart Materials and Structures*, **15**(6):1499-1512. [doi:10.1088/0964-1726/15/6/001]

Tadesse, Y., Zhang, S., Priya, S., 2009. Multimodal energy harvesting system: piezoelectric and electromagnetic. *Journal of Intelligent Material Systems and Structures*, **20**(5):625-632. [doi:10.1177/1045389X08099965]

Tang, L.H., Yang, Y.W., 2012. A multiple-degree-of-freedom piezoelectric energy harvesting model. *Journal of Intelligent Material Systems and Structures*, **23**(14):1631-1647. [doi:10.1177/1045389X12449920]

Tang, L.H., Yang, Y.W., Soh, C.K., 2013. Broadband vibration energy harvesting techniques. Elvin, N., Erturk, A. (Eds.), Advances in Energy Harvesting Methods. Springer, New York, USA, p.17-61.

Wacharasindhu, T., Kwon, J.W., 2008. A micromachined energy harvester from a keyboard using combined electromagnetic and piezoelectric conversion. *Journal of Micromechanics and Microengineering*, **18**(10):104016. [doi:10.1088/0960-1317/18/10/104016]

Wang, H.Y., Shan, X.B., Xie, T., 2012. An energy harvester combining a piezoelectric cantilever and a single degree of freedom elastic system. *Journal of Zhejiang University-SCIENCE A (Applying Physics & Engineering)*, **13**(7):526-537. [doi:10.1631/jzus.A1100344]

Wang, H.Y., Tang, L.H., Shan, X.B., *et al*., 2014. Modeling and performance evaluation of a piezoelectric energy harvester with segmented electrodes. *Smart Structures and Systems*, **14**(2):247-266. [doi:10.12989/sss.2014.14.2.247]

Williams, C.B., Yates, R.B., 1996. Analysis of a micro-electric generator for microsystems. *Sensors and Actuators A: Physical*, **52**(1-3):8-11. [doi:10.1016/0924-4247(96)80118-X]

Yang, B., Lee, C., Kee, W.L., *et al*., 2010. Hybrid energy harvester based on piezoelectric and electromagnetic mechanisms. *Journal of Micro/Nanolithography, MEMS,*

and MOEMS, **9**(2):023002. [doi:10.1117/1.3373516]

Yang, Y.W., Tang, L.H., Li, H.Y., 2009. Vibration energy harvesting using macro-fiber composite. *Smart Materials and Structures*, **18**(11):115025. [doi:10.1088/0964-1726/18/11/115025]

中文概要：

本文题目： 一种两自由度的压电-电磁复合能量收集器

A 2DOF hybrid energy harvester based on combined piezoelectric and electromagnetic conversion mechanisms

研究目的： 对一种两自由度的压电-电磁复合能量收集器进行发电性能研究。

创新要点： 建立了一种两自由度压电-电磁复合能量收集器发电性能的数学模型，该数学模型可以评估两自由度压电-电磁复合能量收集器中压电元件、电磁元件以及系统总输出功率。

研究方法： 对一种两自由度的压电-电磁复合能量收集器进行数学建模，并实验验证数学模型的正确性。基于实验测试得到的系统参数值，理论研究压电元件和电磁元件的机电耦合系数对不同能量收集器发电性能的影响关系，并对几种能量收集器的发电能力进行对比分析。

重要结论： 对于非强耦合（弱或中间耦合）的两自由度机电转换器，复合能量收集器（压电+电磁）具有比单一能量收集器（压电或电磁）更高的发电能力。

关键词组： 振动；复合能量收集；两自由度模型；压电；电磁